Dissecting the Mechanisms Underlying the Cytokine Release Syndrome (CRS) Mediated by T-Cell Bispecific Antibodies

Gabrielle Leclercq-Cohen[1], Nathalie Steinhoff[1], Llucia Albertí Servera[2], Sina Nassiri[2], Sabrina Danilin[2], Emily Piccione[3], Emilio Yángüez[1], Tamara Hüsser[1], Sylvia Herter[1], Stephan Schmeing[1], Petra Gerber[1], Petra Schwalie[2], Johannes Sam[1], Stefanie Briner[1], Sylvia Jenni[1], Roberta Bianchi[1], Marlene Biehl[1], Floriana Cremasco[1], Katerina Apostolopoulou[1], Hélène Haegel[2], Christian Klein[1], Pablo Umaña[1], and Marina Bacac[1]

ABSTRACT

Purpose: Target-dependent TCB activity can result in the strong and systemic release of cytokines that may develop into cytokine release syndrome (CRS), highlighting the need to understand and prevent this complex clinical syndrome.

Experimental Design: We explored the cellular and molecular players involved in TCB-mediated cytokine release by single-cell RNA-sequencing of whole blood treated with CD20-TCB together with bulk RNA-sequencing of endothelial cells exposed to TCB-induced cytokine release. We used the *in vitro* whole blood assay and an *in vivo* DLBCL model in immunocompetent humanized mice to assess the effects of dexamethasone, anti-TNFα, anti-IL6R, anti-IL1R, and inflammasome inhibition, on TCB-mediated cytokine release and antitumor activity.

Results: Activated T cells release TNFα, IFNγ, IL2, IL8, and MIP-1β, which rapidly activate monocytes, neutrophils, DCs, and NKs along with surrounding T cells to amplify the cascade further, leading to TNFα, IL8, IL6, IL1β, MCP-1, MIP-1α, MIP-1β, and IP-10 release. Endothelial cells contribute to IL6 and IL1β release and at the same time release several chemokines (MCP-1, IP-10, MIP-1α, and MIP-1β). Dexamethasone and TNFα blockade efficiently reduced CD20-TCB–mediated cytokine release whereas IL6R blockade, inflammasome inhibition, and IL1R blockade induced a less pronounced effect. Dexamethasone, IL6R blockade, IL1R blockade, and the inflammasome inhibitor did not interfere with CD20-TCB activity, in contrast to TNFα blockade, which partially inhibited antitumor activity.

Conclusions: Our work sheds new light on the cellular and molecular players involved in cytokine release driven by TCBs and provides a rationale for the prevention of CRS in patients treated with TCBs.

See related commentary by Luri-Rey et al., p. 4320

Introduction

In the field of cancer immunotherapy, redirecting T-cell cytotoxicity toward tumor cells is a promising approach for the treatment of various types of cancer. T-cell bispecific antibodies (TCB) are a class of T-cell engagers, which activate T cells by engaging the CD3ε chain of the T-cell receptor and simultaneously binding to tumor-associated antigens on-target cells. This enables the formation of immunologic synapses where the release of the pore-forming cytolytic protein (perforin) and of the cytotoxic granule (granzyme B) induce target cell killing (1–4). We have previously described several TCBs including CEA-TCB (cibisatamab), CD20-TCB (glofitamab), WT1-TCB (a TCR-like TCB), EGFRVIII-TCB, and BCMA-TCB, which are engineered with the same 2:1 format enabling potent T-cell activation and tumor cell killing (1–3, 5–9). Importantly, TCBs directed against hematologic tumors demonstrated positive clinical outcomes. Among them, glofitamab (CD20-TCB) has shown promising activity in diffuse large B-cell lymphoma (DLBCL) and other non-Hodgkin lymphoma (NHL) patients (7, 10–12).

Despite promising activity, on-target activation of T cells is associated with an intrinsic risk of cytokine release syndrome (CRS), one of the most common adverse events associated with the treatment with T-cell–engaging therapies (13–17). CRS is characterized by cytokine release resulting from an overactivation of both T cells and innate immune cells, causing symptoms, which include fever, hypotension, and respiratory deficiency, and in the worst case, multiorgan failure (13, 18, 19). The American Society for Transplantation and Cellular Therapy (ASTCT) consensus classifies CRS into different grades based on clinical symptoms (e.g., fever, hypotension, and hypoxia). High-dose glucocorticoids and/or IL6R blockade (tocilizumab) can be utilized to alleviate symptoms (13, 18). In the specific case of T-cell engagers, step-up dosing (SUD) or fractionated dosing regimens are widely used in the clinic to lower the risk of CRS (10). Target cell predepletion approaches may also be applied in case of B-cell targeting T-cell engagers to reduce the amount of circulating and lymphoid tissue-resident CD20/CD19-expressing B cells and subsequently reduce the systemic on-target cytokine release by T-cell–engaging therapies directed against B-cell malignancies. One clinically

[1]Roche Pharma Research and Early Development, Roche Innovation Center Zurich, Roche Pharma Research and Early Development, Schlieren, Switzerland. [2]Roche Pharma Research and Early Development, Roche Innovation Center Basel, Roche Pharma Research and Early Development, Basel, Switzerland. [3]Oncology Biomarker Development, Genentech, San Francisco, California.

G. Leclercq-Cohen and N. Steinhoff share first authorship of this article.

Corresponding Author: Gabrielle Leclercq-Cohen, Pharma Research and Early Development, Roche (Switzerland), Wagistrasse 10, Schlieren 8952, Switzerland. E-mail: gabrielle.leclercq-cohen@roche.com

Clin Cancer Res 2023;29:4449–63

doi: 10.1158/1078-0432.CCR-22-3667

Translational Relevance

Despite the promising clinical activity of T-cell bispecific antibodies (TCB), cytokine release syndrome (CRS) remains a common dose-limiting safety liability associated with TCB treatment. We provide a mechanistic and kinetic understanding of TCB-mediated cytokine release. In particular, we dissect the contribution of immune cells using scRNA-sequencing of human whole blood treated with a B-cell targeting TCB and of endothelial cells using bulk RNA-sequencing. We highlight the molecular players involved in CRS together with the timing of their upregulation in different immune cells. In parallel, we present the comparative assessment of clinically available therapeutic approaches for the mitigation of CRS, including IL6R blockade (tocilizumab), TNFα blockade (adalimumab), IL1R blockade (anakinra), inflammasome inhibition, and dexamethasone in the *in vitro* whole blood assay system and in a diffuse large B-cell lymphoma (DLBCL) *in vivo* model in humanized NSG mice. These provide experimental evidence for the efficient mitigation of CRS in patients treated with TCBs.

relevant example is the pretreatment with obinutuzumab (Gpt) in combination with SUD of glofitamab (CD20-TCB), which lowers the rate and severity of CRS (3, 7).

In spite of these management strategies, CRS still occurs in some patients treated with TCBs. This highlights the need to better characterize this complex clinical syndrome in the context of T-cell engagers and to identify mitigation strategies that reduce cytokine release while retaining treatment efficacy. In this work, we first aimed to dissect the kinetics of events to identify the early players that "trigger" cytokine release along with the ones that "amplify" the signal later on. We used single-cell RNA-sequencing (scRNA-seq) of whole blood following incubation with CD20-TCB, targeting CD20-expressing B cells. This model system aims to reflect the kinetics of cytokine release observed in DLBCL patients after the first CD20-TCB dose. We focused on identifying the key molecular players in immune cells present in the human whole blood, including neutrophils, which are among the most abundant (yet poorly studied due to their fragility) cytokine-secreting immune cell population in blood that is lost during PBMC isolation (20). In addition, we also conducted bulk RNA-sequencing of endothelial cells exposed to cytokine-rich supernatants from a T-cell–dependent cytotoxicity assay to explore their contribution to cytokine release. In parallel, we assessed the effects of the known CRS mitigation approaches, including dexamethasone, adalimumab (anti-TNFα), tocilizumab (anti-IL6R), and anakinra (anti-IL1R) on cytokine release and efficacy of CD20-TCB in both, whole blood assays and DLBCL tumor-bearing humanized mice (4, 18, 20–23). In parallel, we also investigated the effects of an inflammasome inhibitor (NLRP3 inhibitor), given the promising activity in alleviating severe symptoms after COVID-19 infections (24). This enabled a comprehensive assessment of the different mitigation approaches on the key molecular players involved in CRS, in addition to evaluating the sequence of events of T-cell engager-mediated cytokine release.

Materials and Methods

Antibodies and compounds

2+1 T-cell bispecific antibodies are IgG1-based with bivalent binding entities to a target antigen and monovalent binding to the CD3ε chain of the T-cell receptor. They have a silent Fc region engineered with a P329G LALA mutation, which prevents binding to the FcγR. DP47-TCB, used as an untargeted-TCB control, has the same IgG1-based format but bears two nonbinding active binders in place of the target antigen binders. Obinutuzumab (Gazyva), CD20-TCB, DP47-TCB, and CEA-TCB were produced internally. The commercial compounds adalimumab, anakinra, and tocilizumab were used to block TNFα, IL1Ra, and IL6 signaling, respectively. The NLRP3 inhibitor (MCC950) was purchased from Sigma-Aldrich. Dexamethasone was purchased from Sigma-Aldrich.

Cell lines

MKN45 (DMSZ) is a human gastric cancer cell line used as target cells in TDCC assays with CEA-TCB. MKN45 cells are adherent cells, which were harvested with Trypsin (Gibco) and were passaged twice per week at a density of 60 000 cell/cm^2 in RPMI Glutamax (Gibco) containing 10% FBS (Gibco).

OCI-Ly18 (DMSZ) is a human DLBCL cell line. OCI-Ly18 was passaged twice per week at a density of 0.6×10^6 cells/mL in RPMI Glutamax (Gibco) containing 10% FBS (Gibco).

Cell lines are routinely authenticated by short tandem repeat profiling. Upon receipt, cells were expanded and frozen; cells were not passaged for more than 6 months after resuscitation. No further authentication of these cell lines was conducted.

Whole blood assays (WBA)

Human fresh blood was collected from anonymous healthy volunteers through the Roche internal employee donation program, in accordance with the declaration of Helsinki. Whole blood (190 μL) was incubated with a dose titration of CD20-TCB (5 μL) in the presence and absence of cytokine/cytokine receptor blocking antibodies (5 μL). At the assay endpoint, 60 μL of serum was collected for cytokine measurements and 20 μL of blood was collected for immune phenotyping by flow cytometry.

Red blood cell magnetic isolation

Total leukocytes were isolated from fresh whole blood by magnetic removal of RBCs using the EasySep RBC depletion kit (Stemcell). Fresh whole blood was diluted 1:2 in PBS with 6 mmol/L EDTA. 10 mL of diluted fresh whole blood was incubated with beads targeting RBCs (50 μL/mL of undiluted blood volume) in a 14-mL polystyrene tube (BD) using a magnetic tube holder (EasyEights, Stemcell) for 5 minutes at RT. The cell suspension was carefully transferred to a new 14-mL polystyrene tube. RBC magnetic isolation was then repeated three times (5 minutes, RT). The clear yellowish cell suspension was collected and placed for 5 minutes in the magnetic tube holder to remove the remaining magnetic beads, and washed twice with PBS by centrifugation at 800 rpm, for 10 minutes (RT) to eliminate the platelets.

T-cell–dependent cytotoxicity assay

Peripheral blood mononuclear cells were purified from Buffy Coats from the Blutspendezentrale Zürich by conventional Histopaque gradient (Sigma-Aldrich). Suspension tumor target cells (MKN45) were harvested and resuspended at 0.3×10^6 cells / mL in assay medium (RPMI-1640, 10% FCS, 1% Glutamax). 100 μL/well of target cells (30,000 cells/well) were seeded into 96-flat-bottom plates for 24 hours at 37°C, 5% CO_2 in the incubator. 50 μL (300,000 cells) of a 6.00×10^6 cells/mL PBMCs stock solution were added to the wells containing the target cells (approximate E:T ratio of 10:1). CEA-TCB was prepared in assay medium and was added to the wells containing the target cells

(50 μL, final end concentration: 4 nmol/L). The assay plates were incubated for 48 hours at 37°C, 5% CO_2 in the incubator. Supernatants were then transferred to human umbilical endothelial cells (HUVEC).

Target cell killing: LDH release

CytoTox-Glo (Promega) cytotoxicity assay was used to measure target cell killing. 75 μL supernatants were collected in a 96-well white plate and 25 μL of CytoTox-Glo reagents were added in each well. The plate was agitated for 15 minutes, 600 rpm, RT, and luminescence was measured using a PerkinElmer plate reader.

Bulk RNA-sequencing of HUVECs

HUVECs were seeded in 6-well plates (145K cells/well), let adhere overnight, and stimulated with conditional media from the TCB killing experiment. The medium from the cells was aspirated, and cells were washed with PBS. Cells were lysed on the wells with 350 μL of RTL buffer. Cell lysates were collected with the help of a scraper, transferred to Eppendorf tubes, and frozen at −80°C prior to continuing with the RNA extraction following the manufacturer's instructions (QIAGEN RNeasy Mini Kit). The RNA concentration was quantified using a Nanodrop instrument, and the quality of the preparations (RIN) was evaluated using an Agilent BioAnalyzer. Libraries were prepared using the Illumina TruSeq Stranded mRNA kit following the recommended instructions and quantified with the qPCR KAPA Library Quantification kit (KAPA Biosystems). The fragment size distribution was evaluated with an Agilent Tapestation. The libraries were sequenced in an Illumina NovaSeq6000 instrument (R1:51, i7:8, i5:8, R2:51) with a targeted depth of 30 Mio paired reads per sample. A comparison between HUVECs incubated with CEA-TCB supernatants and HUVECs incubated with DP47-TCB (negative control) supernatants was conducted to identify differentially expressed genes.

In vivo studies

Mice were maintained under specific pathogen-free conditions with daily cycles of 12-hour light/12-hour darkness according to international (Federation of European Laboratory Animal Science Associations) and national (Gesellschaft für Versuchstierkunde/Society of Laboratory Animal Science (GV-Solas) and Tierschutzgesetz (TierSchG) guidelines. The study protocol was reviewed and approved by the local government (license ZH225-17). CD20-expressing OCI-Ly18 cells were cultured at 37°C in a water-saturated atmosphere with 5% CO_2. Cells were harvested, washed once with RPMI, and resuspended in RPMI admixed with 50% Matrigel at 5×10^7 cells/mL. 100 μL of this solution was injected subcutaneously into the flank of female stem cell–humanized NSG mice (HSC-NSG, 5×10^6 OCI-LY18 cells) subcutaneously tumor volumes were calculated from caliper measurements conducted 2–3 times per week. Treatment started when the tumor volumes reached approximately 100 to 150 mm^3, which was 15 days after tumor cell injection. Mice were pretreated with 30 mg/kg obinutuzumab (Gazyva; Gpt), 3 days prior to the first administration of CD20-TCB or vehicle. Mice received a total of 3 cycles of CD20-TCB with an SUD ranging from 0.5 mg/kg to 1 mg/kg to 2 mg/kg. Obinutuzumab and CD20-TCB were administered intravenously (i.v.). Adalimumab (25 mg/kg, i.v.) and tocilizumab (10 mg/kg. i.v.) were given 1 day and 1 hour prior to each CD20-TCB treatment. Dexamethasone (1 mg/kg) was given 1 hour prior to each CD20-TCB therapy. Anakinra (10 mg/kg, i.v.) and NLRP3 inhibitor (20 mg/kg, i.p.) were administered 1 hour before and 4 hours and 1 day after the first CD20-TCB treatment as well as 1 hour before and 4 hours after the second CD20-TCB treatment. Compound dilutions were daily prepared in histidine buffer prior to therapy. Blood was collected by tail-vein bleedings 3 hours and 24 hours after the first CD20-TCB treatment.

Flow-cytometry analysis

20 μL whole blood was lysed twice (10 minutes, RT) with 200 μL lysis buffer (BD Pharm Lyse), and washed with PBS. Cells were stained with a LIVE/DEAD Fixable Aqua Dead dye (Thermo Fisher Scientific) according to the manufacturer's instructions. Surface staining was performed with the antibodies listed in Supplementary Table S1.

Total leukocytes obtained after magnetic depletion of red blood cells were stained with a LIVE/DEAD Fixable Aqua Dead dye (Thermo Fisher Scientific) according to the manufacturer's instructions. Surface staining was performed with the antibodies listed in Supplementary Table S2.

HUVECs were harvested and stained with a LIVE/DEAD a LIVE/DEAD Fixable Aqua Dead dye (Thermo Fisher Scientific) according to the manufacturer's instructions. Surface staining was performed with the antibodies listed in Supplementary Table S3.

Tumor samples were dissociated into cell suspensions using the gentleMACS Octo Dissociator (Miltenyi Biotec) and digested with DNAse and Liberase. Cell suspensions were stained with LIVE/DEAD Fixable Blue Dead dye (Thermo Fisher Scientific) to exclude dead cells according to the manufacturer's instructions. Surface staining was performed with the antibodies listed in Supplementary Table S4.

The final cell suspensions were washed, resuspended in FACS buffer, and acquired using a BD LSR Fortessa cell analyzer (BD).

Multiplex cytokine analysis

Cytokines were analyzed in the serum collected from WBA or from humanized mouse blood (stored at −80°C) using the Luminex technology with a Bio-Plex Pro Human Chemokine Panel (Bio-Rad). Prediluted serum was incubated with beads for 1 hour and then centrifuged at 800 rpm. The plate was washed with wash buffer and detection antibodies were added for 1 hour before centrifugation at 800 rpm. The plate was washed again, and streptavidin was added for 1 hour before centrifugation at 800 rpm. After another washing, samples were resuspended in assay buffer before being measured by fluorescence reading using a Luminex plate reader from Bio-Rad. Data were analyzed using the Bio-Rad Bio-Plex Software.

Cytokine measurement in clinical samples

Blood samples were collected from patients at predefined time points per clinical protocol during the course of treatment. All patients provided written informed consent. The trial was approved by each center's ethics committee or institutional review board and was performed in compliance with the Declaration of Helsinki and the International Conference on Harmonization Guidelines for Good Clinical Practice. Plasma samples were prepared for cytokine (IFNγ, TNFα, and IL6) analysis using validated multiplex immunoassays on a ProteinSimple Ella platform (Microcoat Biotechnologie GmbH).

Data analysis and representation

Flow-cytometry data were analyzed using FlowJo V10. Cytokine data were analyzed using the Bio-Plex software from Bio-Rad. GraphPad Prism 8 was used to generate the graphs, for statistical analysis and to calculate the area under the curve (AUC) for dose–response experiments. The respective statistical tests used are indicated in the figure legends for each experiment.

scRNA-seq of whole blood

As previously described, whole blood from 4 donors was treated with 0.2 μg/mL CD20-TCB, or incubated in the absence of CD20-TCB (20). At baseline (before the addition of TCB) and assay endpoints (2, 4, 6, and 20 hours), blood was collected for total leukocyte isolation using EasySep red blood cell depletion reagent (Stemcell). Briefly, cells were counted and processed for scRNA-seq using the BD Rhapsody platform. To load several samples on a single BD Rhapsody cartridge, sample cells were labeled with sample tags (BD Human Single-Cell Multiplexing Kit) following the manufacturer's protocol prior to pooling. Briefly, 1×10^6 cells from each sample were resuspended in 180 μL FBS Stain Buffer (BD, PharMingen) and sample tags were added to the respective samples and incubated for 20 minutes at RT. After incubation, 2 successive washes were performed by addition of 2 mL stain buffer and centrifugation for 5 minutes at 300 × *g*. Cells were then resuspended in 620 μL cold BD Sample Buffer, stained with 3.1 μL of both 2 mmol/L Calcein AM (Thermo Fisher Scientific) and 0.3 mmol/L Draq7 (BD Biosciences) and finally counted on the BD Rhapsody scanner. Samples were then diluted and/or pooled equally in 650 μL cold BD Sample Buffer. The BD Rhapsody cartridges were then loaded with up to 40,000 to 50,000 cells. Single cells were isolated using Single-Cell Capture and cDNA Synthesis with the BD Rhapsody Express Single-Cell Analysis System according to the manufacturer's recommendations (BD Biosciences). cDNA libraries were prepared using the Whole-Transcriptome Analysis Amplification Kit following the BD Rhapsody System mRNA Whole-Transcriptome Analysis (WTA) and Sample Tag Library Preparation Protocol (BD Biosciences).

Indexed WTA and sample tags libraries were quantified and quality controlled on the Qubit Fluorometer using the Qubit dsDNA HS Assay, and on the Agilent 2100 Bioanalyzer system using the Agilent High Sensitivity DNA Kit. Sequencing was performed on a Novaseq 6000 (Illumina) in paired-end mode (64-8-58) with Novaseq6000 S2 v1 or Novaseq6000 SP v1.5 reagents kits (100 cycles).

scRNA-seq data analysis

As previously described, sequencing data were processed using the BD Rhapsody Analysis pipeline (v 1.0 https://www.bd.com/documents/guides/user-guides/GMX_BD-Rhapsody-genomics-informatics_UG_EN.pdf) on the Seven Bridges Genomics platform. Briefly, read pairs with low sequencing quality were first removed, and the cell label and UMI were identified for further quality check and filtering. Valid reads were then mapped to the human reference genome (GRCh38-PhiX-gencodev29) using the aligner Bowtie2 v2.2.9, and reads with the same cell label, same UMI sequence, and same gene were collapsed into a single raw molecule while undergoing further error correction and quality checks. Cell labels were filtered with a multistep algorithm to distinguish those associated with putative cells from those associated with noise. After determining the putative cells, each cell was assigned to the sample of origin through the sample tag (only for cartridges with multiplex loading). Finally, the single-cell gene-expression matrices were generated and a metrics summary was provided.

After preprocessing with BD's pipeline, the count matrices and metadata of each sample were aggregated into a single data object and loaded into the besca v2.3 pipeline for the scRNA-seq analysis (25). First, low-quality cells with less than 200 genes, less than 500 counts, or more than 30% of mitochondrial reads were filtered. This permissive filtering was used in order to preserve the neutrophils. Potential multiplets (cells with more than 5,000 genes or 20,000 counts), and genes expressed in less than 30 cells were further excluded. Normalization to log-transformed UMI counts per 10,000 reads [log(CP10K + 1)] was applied before downstream analysis. After normalization, the technical variance was removed by regressing out the effects of total UMI counts and percentage of mitochondrial reads, and gene expression was scaled. The 2,507 most variable genes (with a minimum mean expression of 0.0125, a maximum mean expression of 3, and a minimum dispersion of 0.5) were used for principal component analysis (PCA). Finally, the first 50 PCs were used as input for calculating the 10 nearest neighbors and the neighborhood graph was then embedded into the two-dimensional space using the UMAP algorithm) (https://doi.org/10.48550/arXiv.1802.03426). Cell clustering was performed using the Leiden algorithm (https://www.nature.com/articles/s41598-019-41695-z) at a resolution of 2 (26).

Cell-type annotation was performed using the Sig-annot semiautomated besca module, which is a signature-based hierarchical cell annotation method (25). The used signatures, configuration, and nomenclature files can be found at https://github.com/bedapub/besca/tree/master/besca/datasets.

Finally, cell types of interest were selected in order to generate further visualizations, such as the expression level of selected cytokines across conditions, by using a custom script with mainly besca and scanpy functions.

Enrichment pathway analysis

Differential expression analysis was performed by using the Wilcoxon test across treatment time points (1 vs. all) for the selected cell types. Only genes with >25% fraction positive in at least one group were considered. A gene was defined as differentially expressed when having a $P_{adj} < 0.05$ and a linear absolute fold change >2. In order to exclude the incubation effect, differentially expressed genes among control samples were filtered out. Next, using the upregulated genes at each timepoint and cell type, pathway enrichment analysis using the enrichr package and the following libraries: GO_Biological_Process_2021, GO_Molecular_Function_2021, KEGG_2021_Human, Reactome_2016, WikiPathways_2019_Human was performed (27). A GO term or pathway was considered enriched when at least 5 genes were present and $P_{adj} < 0.05$. Finally, significantly enriched pathways of interest were selected, and the per-cell score was computed using the scanpy method score_genes with default parameters selected. For the latter, the pathway genes that were identified as differentially expressed at any time point or cell type of interest were used. The score distribution was visualized in ridge plots generated with custom scripts.

Data availability

The bulk RNA-seq data generated and analyzed in this study are available in Gene-Expression Omnibus at GSE234676. The scRNA-seq data generated and analyzed in this study are available in Figshare at https://doi.org/10.6084/m9.figshare.23499192.v1.

Other data generated in this study are available upon request from the corresponding author.

Additional methods are described in the Supplementary Methods S1 file.

Results

WBA with CD20-TCB recapitulates T-cell activation, cytokine, and chemokine release

We used a whole blood assay system to explore the onset of on-target T-cell activation, target cell depletion, cytokine, and chemokine release induced by CD20-TCB. In the whole blood assay model system, the presence of healthy $CD20^+$ B cells induces on-target activity of

CD20-TCB and allows to study the abundant neutrophil population, which is lost during PBMC isolation, in addition to all the other cell types present in PBMCs. Whole blood from two healthy donors (donors 3 and 4 from the following scRNA-seq experiment) was incubated with CD20-TCB for 2, 6, and 20 hours to evaluate the early kinetics of cytokine release. As early as 2 hours following treatment with CD20-TCB, we detected B-cell depletion and activation of T cells, as indicated by the percentages of $CD19^+$ B cells and expression of CD25 and CD69 activation markers on T cells (**Fig. 1A** and **B**). The highest level of target cell lysis along with the strongest T-cell activation was observed at 20 hours (**Fig. 1A** and **B**). Along with this, elevated concentrations of IFNγ, TNFα, IL2, IP-10, MCP-1, MIP-1α, MIP-1β, IL1β, and IL1Ra were detected at 6 hours of treatment in the serum of these assays, whereas IL6 and IL8 were first detected at 6 hours and most elevated at 20 hours within the experimental time frame (**Fig. 1C**; ref. 26; Supplementary Fig. S1A). At longer incubation time, most cytokines accumulated in the serum with the exception of IL8 and IL10, which decreased, suggesting that they may be consumed (Supplementary Fig. S1B). Similar to our *in vitro* system, cytokine kinetics were evaluated in relapsed/refractory DLBCL patients treated with CD20-TCB monotherapy in the NP30179 (NCT03075696) clinical study. Cytokine kinetics in patients treated with 2.5 mg CD20-TCB were similar to our *in vitro* WBA system with IFNγ and TNFα reaching peak levels by 6 hours after infusion of CD20-TCB and delayed kinetics of IL6 not peaking until 20 hours following infusion (**Fig. 1D**).

scRNA-seq of the human whole blood treated with CD20-TCB reveals a strong phenotypic change in T cells, neutrophils, and monocytes

We further aimed to explore the sequence of events involved in TCB-induced cytokine release. To this end, we conducted scRNA-seq of healthy donor human whole blood before (pre-TCB) and after 2, 4, 6, and 20 hours of incubation with 0.2 μg/mL CD20-TCB using the BD Rhapsody platform (**Fig. 2A**). ScRNA-seq of untreated whole blood (incubated under the same culture conditions as CD20-TCB–treated samples) was performed at 2, 6, and 20 hours to consider the potential impact of *ex vivo* culture (**Fig. 2A**). UMAP plots generated by scRNA-seq data analysis reveal different clusters of immune cells in whole blood, including $CD4^+$ T cells, $CD8^+$ T cells, NK cells, dendritic cells (DC), B cells, monocytes and, importantly, a large population of neutrophils (**Fig. 2B**). The proportion of cells identified by scRNA-seq reflects similar ratios measured by flow cytometry in the same samples (**Fig. 2B**; Supplementary Fig. S2A–S2C). In addition to the main immune cell populations, and in line with the mode of action of CD20-TCB that bridges T cells to B cells, we also identified a time-dependent cluster of interacting B and T cells in treated samples, where B and T-cell markers were coexpressed (**Fig. 2B** and **C**; Supplementary Fig. S3A–S3E). Importantly, there were no quantitative changes in the frequency of the $CD4^+$ T cells, $CD8^+$ T cells, monocytes, or neutrophils within the experimental time frame (2–20 hours of treatment) for all 4 donors, allowing us to focus on immune cell activation states, pathways, and the key molecular players involved therein (**Fig. 2C**). The comparison of single cells from the treated and untreated samples shown in the UMAP plots of **Fig. 2D** suggests that CD20-TCB treatment leads to a shift in T-cell, monocyte, and neutrophil state starting at 4 hours, with the most pronounced changes observed in monocyte and neutrophil populations at 20 hours. At 4 hours, treated cells were compared with the cells from the pretreatment sample (0 hours). To confirm this observation, we plotted the multidimensional scaling plots showing each sample per cell type colored by cell type or by treatment and time point (Supplementary Fig. S4A–S4B). Using a linear mixed model to quantify and interpret the contribution of treatment, time point, and their interaction to gene-expression variation, we confirmed that the largest transcriptomic changes induced by CD20-TCB treatment over time were observed in neutrophils, monocytes, $CD4^+$, and $CD8^+$ T cells (**Fig. 2E**; ref. 28). Altogether, these data demonstrate that $CD4^+$ and $CD8^+$ T cells, neutrophils, and monocytes are the most affected cell populations by CD20-TCB treatment.

scRNA-seq of whole blood treated with CD20-TCB highlights the cellular source of inflammatory pathways and molecular players together with the timing of their upregulation in the cytokine release cascade

We further investigated the contribution of $CD4^+$ and $CD8^+$ T cells, neutrophils, and monocytes to the inflammatory response induced by CD20-TCB. Hallmark enrichment pathway analysis outlined the cascade of activation events in CD20-TCB-mediated immune cell activation. In particular, it revealed the enrichment of TNFα signaling via NF-κB, IL6 JAK/STAT3, IFNγ response and inflammatory response signaling pathways in $CD4^+$ T cells, $CD8^+$ T cells, monocytes, and neutrophils as early as 2–4 hours after treatment (**Fig. 3A**). Interestingly, the enrichment of those pathways was stronger in monocytes and neutrophils compared with T cells 2–4 hours after treatment and was the strongest 20 hours after treatment. This suggests that monocytes and neutrophils react strongly and further amplify the inflammation signal in peripheral blood (**Fig. 3A**). The enrichment of various GO biological inflammatory pathways in T cells, monocytes, and neutrophils also confirms these findings (Supplementary Fig. S5A–S5D). Because neutrophils are poorly studied by scRNA-seq, we further corroborated their contribution to TCB-mediated inflammation by bulk RNA-sequencing (Supplementary Fig. S6). In line with the scRNA-seq analysis, the bulk RNA-seq data revealed the early enrichment of hallmark pathways, including TNFα signaling via NF-κB, IL6 JAK/STAT3, IFNγ response and inflammatory response pathways (Supplementary Fig. S6).

We next conducted a more detailed analysis of the cell types expressing the key molecular players involved in cytokine release, to gain insight into the timing of their upregulation and involvement in the cytokine cascade. First, the differential gene-expression analysis revealed the cytokine genes induced by CD20-TCB, among which TNF-a (*TNF*), IFNγ (*IFN*), IL1β (*IL1B*), IL6 (*IL6*), IL8 (*CXCL8*), MCP-1 (*CCL2*), MIP-1α (*CCL3*), MIP-1β (*CCL4*), and IP-10 (*CXCL10*) were identified (Supplementary Fig. S7). IFNγ (*IFNG*) gene is specifically induced in T cells ($CD4^+$, $CD8^+$, interacting T, and B cells, MAIT T cells), and to some extent in NK cells, as early as 2 hours after TCB engagement. In contrast, TNFα transcript (*TNF*) is upregulated in numerous immune cells, including $CD8^+$ T cells, MAIT T cells, monocytes, neutrophils, plasmacytoid, and conventional dendritic cells at 2–4 hours (**Fig. 3B–E**; Supplementary Figs. S8A–S8I and S9–S11). Of note, all immune cells also expressed TNFR1a (*TNFRSF1A)*, TNFR1b (*TNFRSF1B*), IFNGR1 (*IFNGR1*), and IFNGR2 (*IFNGR2*) genes, suggesting that TNFα and IFNγ may act in an autocrine and paracrine loop to further amplify immune cell activation via their receptors (Supplementary Fig. S8A–S8I). Monocytes, neutrophils, and moderately conventional dendritic cells appeared to be the main contributors of IL1β and IL8 as demonstrated by the early upregulation IL1β (*IL1B*) and IL8 (*CXCL8*) genes 2 hours after TCB stimulation (**Fig. 3B–E**; Supplementary Fig. S8F–S8I; Supplementary Fig. S10–S11). Interestingly, neutrophils downregulated IL8 receptor genes *CXCR1* and *CXCR3*, indicating that IL8 may

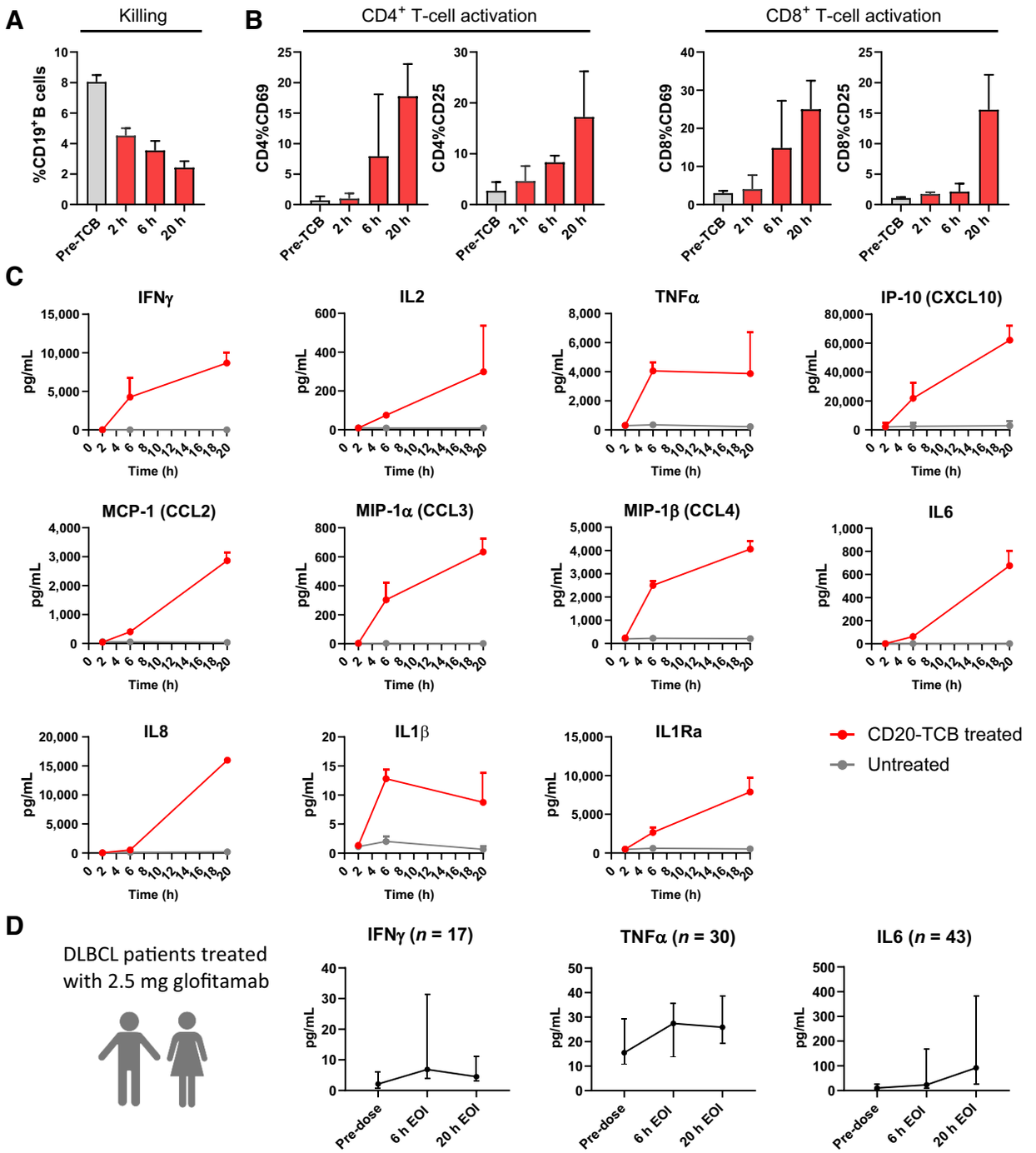

Figure 1.

Kinetics of cytokine release in WBA reflect those observed in DLBCL patients after the first treatment with CD20-TCB. Whole blood from donors 3 and 4 used in the scRNA-seq experiment was incubated in the presence and the absence of 0.2 μg/mL CD20-TCB for 2, 6, and 20 hours. **A,** The proportion of $CD19^+$ B cells among live total leukocytes and (**B**) the expression of CD69 and CD25 on $CD4^+$ and $CD8^+$ T cells was measured by flow cytometry for 2 donors before and after treatment with CD20-TCB for 2, 6, and 20 hours. Means of $n = 2$ donors + SD. **C,** The levels of cytokines were measured by Luminex in serum from whole blood assay untreated or treated with 0.2 μg/mL at 2, 6, and 20 hours. Means of $n = 2$ donors + SD. **D,** Plasma samples from biomarker-evaluable DLBCL patients treated with 2.5 mg of glofitamab were evaluated for IFNγ ($n = 17$), TNFα ($n = 30$), or IL6 ($n = 43$). Median with interquartile range. 6 hours EOI, 6 hours after end of infusion; 20 hours EOI, 20 hours after end of infusion.

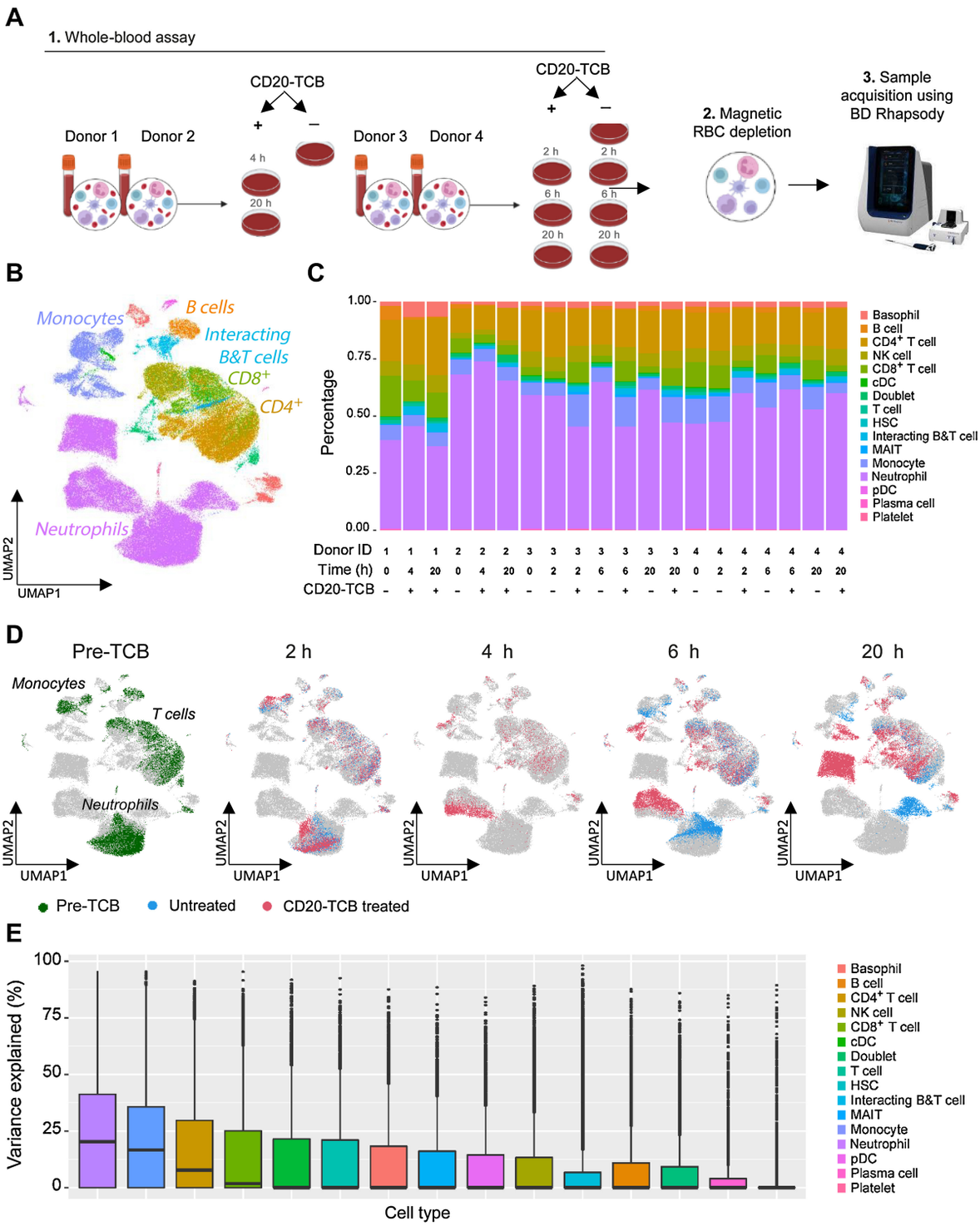

Figure 2.

ScRNA-sequencing of whole blood treated with CD20-TCB reveals an early phenotypic change in T cells, monocytes, and neutrophils. **A,** scRNA-seq of whole blood was performed using the BD Rhapsody platform at baseline (donors 1, 2, 3, and 4) and 2 hours (donors 3 and 4), 4 hours (donors 1 and 2), 6 hours (donors 3 and 4), and 20 hours (donors 1, 2, 3, and 4) after treatment with 0.2 μg/mL CD20-TCB. **B,** UMAP plot of immune cells colored by cell types reveals a large proportion of neutrophils. **C,** Stacked barplot with cell type proportions for each sample analyzed for scRNA-seq. **D,** UMAP plots of immune cells colored by treatment. The UMAP plots show single cells from all time points in gray, cells from baseline samples in green, cells from treated samples at 2-, 4-, 6-, and 20-hour time points in pink, and cells from untreated samples at 2-, 4-, 6-, and 20-hour time points in blue. Each dot represents one cell. **E,** Box plot representing the percentage of variance in gene expression attributed to treatment-induced changes between time points across different cell types.

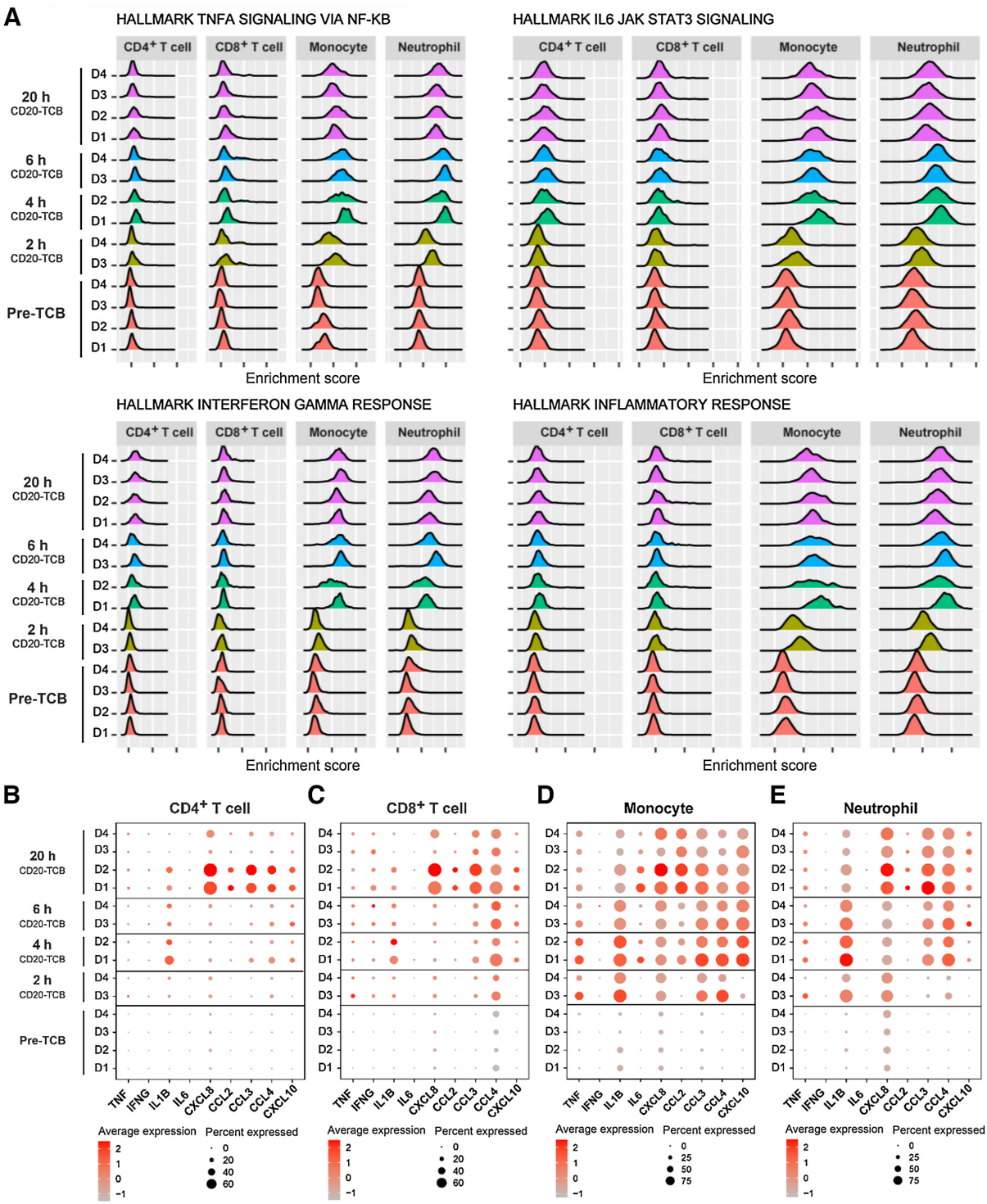

Figure 3.

The hallmark pathway analysis and cytokine expression reveal that myeloid cells are indirectly amplifying proinflammatory cytokine release after the initial activation of CD4$^+$ and CD8$^+$ T cells by CD20-TCB. scRNA-seq of whole blood treated with 0.2 μg/mL CD20-TCB was performed using the BD Rhapsody platform at baseline, 2, 4, 6, and 20 hours. **A,** Ridge plots representing the enrichment kinetics of the TNFα signaling via NF-κB, IL6 JAK STAT3, IFNγ response and inflammatory response hallmark pathways in CD4$^+$, CD8$^+$, monocytes, and neutrophils following treatment with CD20-TCB. **B–E,** Dot plots showing the kinetics of gene-expression distribution in (**B**) CD4$^+$ T cells, (**C**) CD8$^+$ T cells, (**D**) monocytes, and (**E**) neutrophils. The expression of TNFα (*TNF*), IFNγ (*IFNG*), IL1β (*IL1B*), IL6 (*IL6*), IL8 (*CXCL8*), MCP-1 (*CCL2*), MIP-1α (*CCL3*), MIP-1β (*CCL4*), and IP-10 (*CXCL10*) is depicted on the graph. The size of the dot represents the percentage of positive cells, and the color scale, the average gene expression.

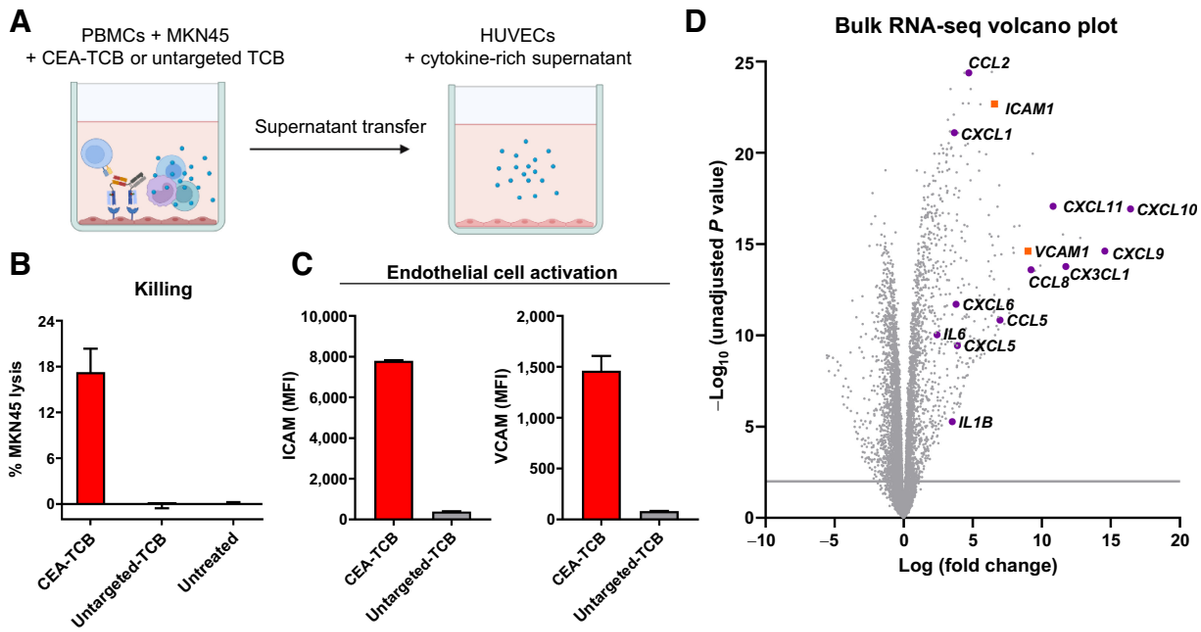

Figure 4.

Activation of endothelial cells following exposure to cytokine-rich supernatants from T-cell–dependent cytotoxicity assay with CEA-TCB. **A,** Assay set-up. Cytokine-enriched supernatants from 48 hours coculture of PBMCs and MKN45 tumor cells with 4 nmol/L CEA-TCB or untargeted-TCB (DP47-TCB, negative control) were incubated on HUVEC cells for 5 hours. **B,** The percentage of MKN45 tumor cell lysis was assessed by LDH release measurements (48 hours). **C,** The expression of ICAM and VCAM on HUVECs was measured by flow cytometry 5 hours after incubation with cytokine-enriched supernatants. **B** and **C,** Means of technical triplicates + SD. **D,** Volcano plot depicting expressed genes in HUVECs following exposure to CEA-TCB–induced cytokine release, each dot represents one gene. The x-axis shows the logarithmic fold change, and the y-axis shows the negative log of the unadjusted *P* value for each gene by comparing samples exposed to CEA-TCB–induced cytokine release to those exposed to untargeted-TCB (negative control) supernatants.

act in an autocrine loop (Supplementary Fig. S8G). $CD4^+$ and $CD8^+$ T cells strongly upregulated the IL8 (*CXCL8*) gene at 20 hours, suggestive of their contribution to IL8 release at later time points. The IL6 (*IL6*) gene is specifically upregulated in monocytes at early time points (2–6 hours) whereas it is expressed by interacting B and T cells together with conventional and plasmacytoid dendritic cells at the later time point of 20 hours (**Fig. 3B–E**; Supplementary Fig. S8F–S8I; Supplementary Fig. S10A–S10C). Only monocytes together with plasmacytoid and conventional dendritic cells upregulated MCP-1 (*CCL2*) gene from 4 hours onward (**Fig. 3B–E**; Supplementary Figs. S8F, S8H, S8I and S10A–S10C). Most blood immune cell subsets upregulated MIP-1α (*CCL3*) and MIP-1β (*CCL4*) genes as early as 2 hours with the exception of neutrophils, plasmacytoid, and conventional dendritic cells that upregulated the genes at 4 hours, suggestive of their slower activation kinetics compared with T cells and monocytes (**Fig. 3B–E**; Supplementary Fig. S7–11). Monocytes and conventional dendritic cells appeared to be the strongest contributors of IP-10 starting from 4 hours of treatment, with interacting B and T cells and plasmacytoid dendritic cells contributing less, as indicated by the IP-10 (*CXCL10*) gene expression (**Fig. 3B–E**; Supplementary Figs. S7, S8, and S10A–S10C). Importantly, all these cytokines and chemokines were detected in the serum of a whole blood assay with CD20-TCB, demonstrating that those are also expressed as proteins, beyond the gene mRNA upregulation (**Fig. 1A**; Supplementary Fig. S1; refs. 29, 30).

Altogether, this analysis recapitulates the initial trigger of IFNγ and TNFα release by $CD4^+$ and $CD8^+$ T cells (2 hours) followed by the strong and rapid amplification of TNFα, IL1β, IL6, IL8, MCP-1, MIP-1α, MIP-1β, and IP-10 by monocytes, neutrophils, and by T cells.

Bulk RNA-sequencing of endothelial cells following exposure to TCB cytokine-rich supernatants highlights their contribution to cytokine release

Because endothelial cells play a major role in the pathophysiology of CRS, we evaluated their contribution to the inflammatory cascade (13). Therefore, HUVECs were incubated with supernatant collected from a killing assay experiment, where tumor cell lysis demonstrated TCB activity (**Fig. 4A** and **B**). Following exposure to the cytokine-rich supernatant, endothelial cells were activated, as shown by the upregulation of adhesion molecules on their surface, including ICAM and VCAM (**Fig. 4C**). In line with this, bulk RNA-seq of endothelial cells revealed the upregulation of *ICAM1* and *VCAM1* genes, confirming the previous observation at the gene mRNA level (**Fig. 4D**). Among the most upregulated genes, we also discerned the upregulation of various chemokines including IP-10 *(CXCL10)*, CXCL9 (*CXCL9)*, fractalkine (*CX3CL1*), MCP-2 *(CCL8)*, RANTES (*CCL5*), MCP-1 (*CCL2*), CXCL1 (*CXCL1*), CXCL5 (*CXCL5*), CXCL6 (*CXCL6*) genes, suggesting that endothelial cells may contribute to the inflammatory cascade and further attract surrounding T cells and myeloid cells with the release of chemoattractant molecules (**Fig. 4D**). In addition, endothelial cells also upregulated IL1β (*IL1B*) and IL6 (*IL6*) genes, indicating that they possibly contribute to the release of these two key CRS cytokines (**Fig. 4D**).

In summary, these data highlight the role of endothelial cells in further mediating the cytokine release cascade with the release of IL6 and IL1β, and, at the same time, attracting peripheral immune cells with the release of various chemokines.

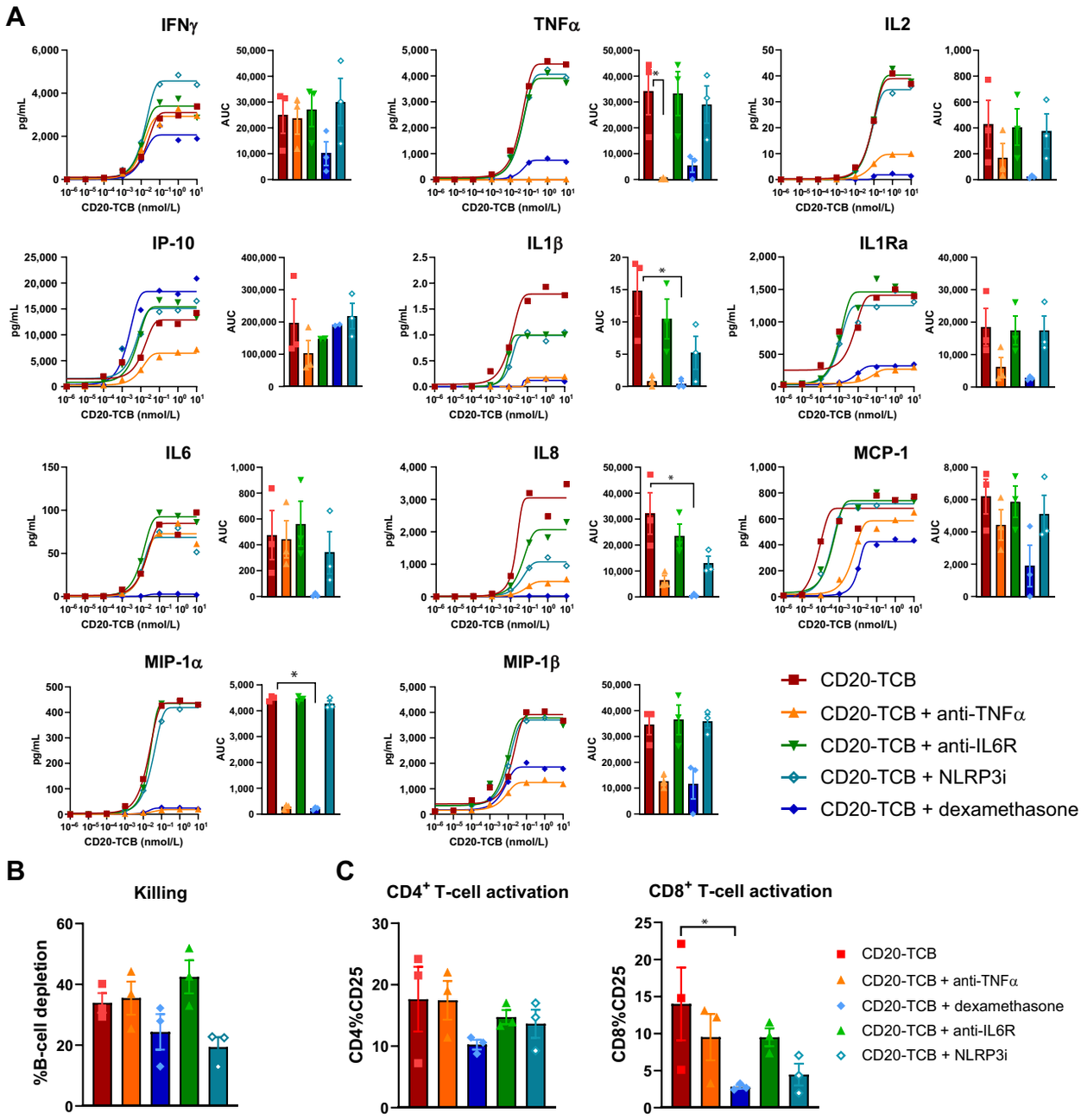

Figure 5.

Effect of TNFα blockade, IL6R blockade, NLRP3 inhibitor, and dexamethasone on CD20-TCB–mediated cytokine release and activity in the human whole blood assay system. WBA with escalating doses of CD20-TCB and TNFα blockade with adalimumab (1 μg/mL), IL6R blockade with tocilizumab (1 μg/mL), NLRP3i (10 μmol/L), and dexamethasone (100 nmol/L). Cytokine levels were measured by Luminex in serum of WBA at 24 hours. **A,** Cytokine release in the serum. Cytokine dose–response curves show data for 1 representative donor. Bar plots show AUC of cytokine dose–response curves for 3 donors with *, $P < 0.05$ by two-way ANOVA. **B,** The killing of $CD19^+$ B cells and (**C**) the expression of CD25 on $CD4^+$ and $CD8^+$ T cells were measured by immune phenotyping of whole blood by flow cytometry after stimulation with 1 nmol/L CD20-TCB (24 hours). **B** and **C,** Means of $n = 3$ donors ± SEM.

Assessment of different mitigation strategies on CD20-TCB–mediated cytokine release and activity in a whole blood assay system

Next, we explored the effects of TNFα blockade (adalimumab), IL6R blockade (tocilizumab), IL1β blockade via inflammasome inhibition (NLRP3 inhibitor), and dexamethasone on CD20-TCB–mediated cytokine release and activity in a whole blood assay. In this *in vitro* system, dexamethasone broadly reduced the secretion of all measured cytokines and chemokines including IFNγ, TNFα, IL2, IL1β, IL1Ra, IL6, IL8, MCP-1, MIP-1α, and MIP-1β (**Fig. 5A**). TNFα

blockade reduced IL2, IP-10, IL1β, IL1Ra, IL8, MCP-1, MIP-1α, and MIP-1β but retained IL6 and IFNγ release, confirming the upstream contribution of TNFα in inducing cytokine release (**Fig. 5A**). The NLRP3 inhibitor reduced IL1β, and to a lower extent, IL6 and IL8 release. In contrast, IL6R blockade did not reduce the overall CD20-TCB–mediated cytokine release, demonstrating that IL6 acts downstream in the cytokine release cascade (**Fig. 5A**).

As the balance between reducing cytokine release and maintaining T-cell cytotoxic activity is key to efficient mitigation strategies, we further assessed their effects on T-cell activation and killing of healthy B cells by flow cytometry. Whereas dexamethasone and the NLRP3 inhibitor minimally interfered with CD20-TCB–induced B-cell depletion, TNFα blockade and IL6R blockade had no effect (**Fig. 5B**). As shown by the expression of CD25 on $CD4^+$ T cells, none of these mitigation approaches interfered with $CD4^+$ T-cell activation (**Fig. 5C**). In contrast, dexamethasone minimally affected CD25 upregulation on $CD8^+$ T cells, suggestive of a partial inhibition of $CD8^+$ T-cell activation (**Fig. 5C**). These data suggest that dexamethasone's capacity to reduce cytokine release may affect T-cell activation under continuous *in vitro* exposure, which was not observed with the other mitigation approaches in the human whole blood assay system.

Assessment of different mitigation strategies on CD20-TCB–mediated cytokine release and activity in a model of DLBCL in humanized mice

In parallel, we used a humanized mouse model of DLBCL subcutaneously engrafted with CD20-expressing OCI-Ly18 tumor cells to assess the effects of the mitigation strategies mentioned above on CD20-TCB–mediated cytokine/chemokine release and antitumor efficacy. In line with the clinical development of CD20-TCB, mice were pretreated with obinutuzumab (Gazyva pretreatment, Gpt) to debulk circulating and tissue-resident B cells and thus reduce the target-dependent cytokine release following the first infusion with CD20-TCB (3, 7, 31). Clinically relevant doses of the different mitigation strategies were given prior to the first administration of CD20-TCB to evaluate their impact on ameliorating cytokine release, which is most pronounced upon the first administration of TCBs (32). Dexamethasone was given in addition prior to the second and the third CD20-TCB administration, whereas anakinra and the NLRP3 inhibitor prior to the second CD20-TCB treatment, to explore their impact upon serial treatment cycles.

We found that dexamethasone and TNFα blockade reduced both T-cell–derived cytokines (IFNγ, IL2, TNFα, IP-10) and myeloid cell–derived cytokines (TNFα, IP-10, IL6, IL1β, IL8, MIP-1β, and MCP-1; **Fig. 6A**). In contrast, the NLRP3 inhibitor and IL1R blockade had a less pronounced effect than dexamethasone and TNFα blockade and partially reduced the levels of IP-10, IL6, and IL1β and, to some extent, IL2, TNFα, IL8, MIP1-β, and MCP-1. In line with *in vitro* findings, tocilizumab induced a milder reduction of cytokine release, with the strongest effect observed on IP-10 (**Fig. 6A**).

Importantly, we found that pretreatment with dexamethasone did not interfere with long-term antitumor activity and minimally interfered with $CD8^+$ T-cell infiltration in tumors collected at experiment termination (**Fig. 6B** and **C**; Supplementary Fig. S12). Similarly, the blockade of IL1R with anakinra, the blockade of IL6R with tocilizumab as well as the NLRP3 inhibitor did not interfere with antitumor efficacy, as indicated by the tumor growth curves and intratumoral $CD8^+$ T-cell infiltration (**Fig. 6B** and **C**; Supplementary Fig. S12). In contrast, the blockade of TNFα with adalimumab negatively affected antitumor activity mediated by CD20-TCB (**Fig. 6B**; Supplementary Fig. S12). The loss of antitumor activity was associated with lower counts of intratumor $CD8^+$ T cells on day 25, suggesting that the blockade of TNFα could possibly prevent intratumoral T-cell infiltration required for TCB activity (**Fig. 6D**). To further investigate how TNFα blockade interferes with CD20-TCB efficacy, we used a 3D *in vitro* system that explores T-cell transmigration (Supplementary Fig. S13A). We found that T-cell transmigration toward cytokine-rich supernatant (derived from a killing assay with CD20-TCB) was strongly reduced in the presence of adalimumab, supporting the important role of TNFα in regulating T-cell infiltration into tumors (Supplementary Fig. S13B).

Collectively, we showed that dexamethasone, NLRP3 inhibitor, IL1R blockade, or IL6R blockade did not interfere with CD20-TCB antitumor activity, with dexamethasone having the strongest effect in reducing the cytokine and chemokine release upon the first TCB administration. In contrast, adalimumab was found to broadly reduce cytokine and chemokine release, but at the same time, negatively affects CD20-TCB antitumor activity possibly by reducing the intratumor T-cell infiltration required for TCB activity.

Discussion

T-cell–engaging therapies, including CAR-T cells and T-cell engagers, are a promising class of cancer immunotherapies capable of redirecting T-cell cytotoxicity to eliminate tumor cells. At the same time, they also drive an inflammatory response, which may be toxic if it develops into a CRS. For CAR-T cells, CRS usually occurs within 10 days after infusion, jointly with CAR-T-cell expansion (33). GM-CSF and IFNγ are described as the main trigger of CRS in the context of CAR-T-cell therapies, by activating monocytes and macrophages, resulting in TNFα, IL6, and IL1β release (34, 35). For T-cell engagers, the risk of CRS is mainly associated with the first dose of treatment and is attenuated after repeated dosing (23, 36, 37). Therefore, we explored the early cascade of events that drive the inflammatory response following T-cell engager treatment before evaluating different prophylactic treatments to mitigate the same.

In particular, we used scRNA-seq of human whole blood treated with CD20-TCB using the BD Rhapsody platform to assess the treatment effects on all cellular components, including the fragile and abundant neutrophils, which are generally lost during PBMCs isolation and thus in general poorly studied in the CRS context. This model system reflects the early kinetics of cytokine release in DLBCL patients treated with 2.5 mg CD20-TCB. Among all cell types present in whole blood, we observed the largest treatment effects in neutrophils, monocytes, $CD4^+$, and $CD8^+$ T cells, evolving from 2 to 20 hours after treatment with CD20-TCB. Hallmark pathway analysis revealed the early enrichment of TNFα-mediated signaling via activation of NF-κB, IL6, JAK/STAT3, IFNγ response, and inflammatory response pathways in $CD4^+$ T cells, $CD8^+$ T cells (2–4 hours), monocytes (2–20 hours), and neutrophils (4–20 hours), suggestive of their early contribution to the proinflammatory response upon CD20-TCB stimulation. We show that CD20-TCB treatment induces activation of T cells that further extends to monocytes (2 hours) and neutrophils (4–20 hours; refs. 20, 23, 38). Of note, the induction of cytokine genes, including TNFα (*TNF*) and IFNγ (*IFNG*), was less pronounced in T cells, suggesting that their upregulation may have been missed at the 2-hour time points or that low levels of T-cell–derived cytokines are needed to activate downstream cell populations. The enrichment of the IL6 JAK/STAT3 signaling pathway in T cells, monocytes, and neutrophils suggests the establishment and further amplification of autocrine and paracrine inflammation loops that increase blood cytokine levels over time (39). The enrichment of TNFα signaling via NF-κB

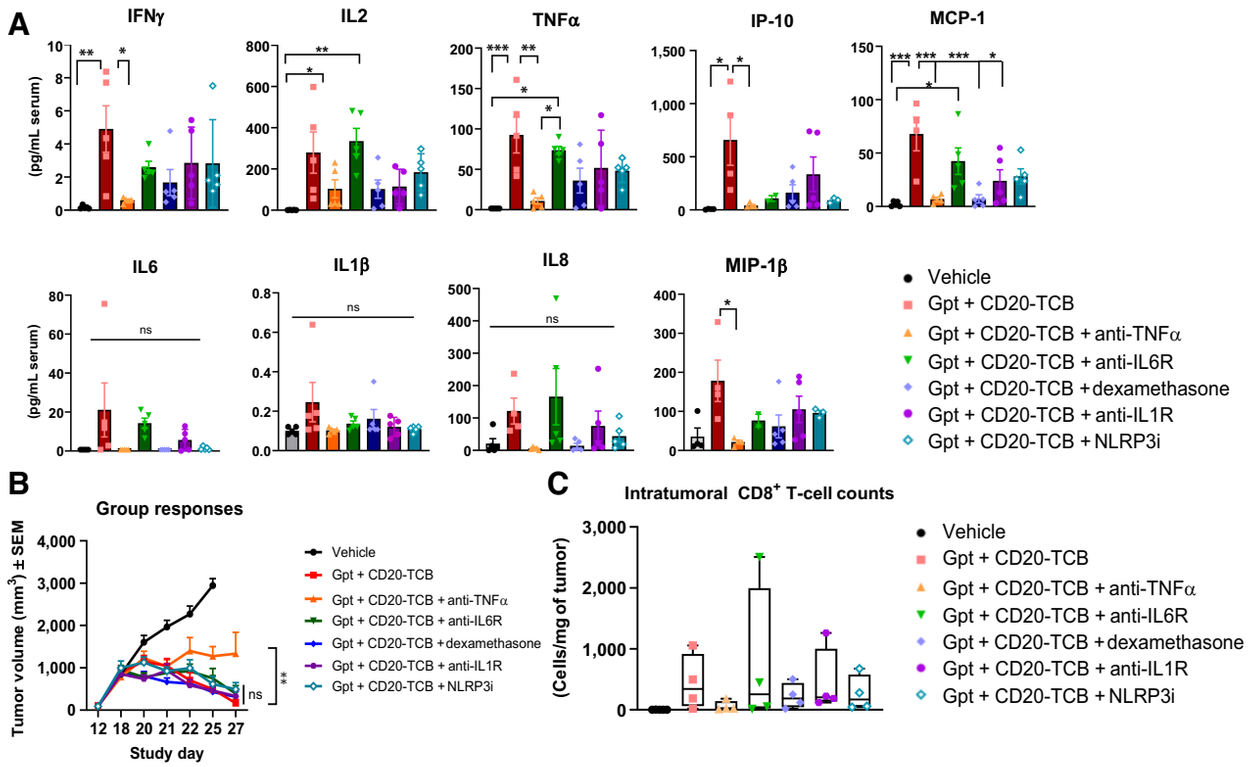

Figure 6.

Effect of TNFα blockade, IL6R blockade, IL1R blockade, NLRP3i, and dexamethasone on CD20-TCB–mediated cytokine release and efficacy in a model of diffused large B-cell lymphoma in humanized mice. OCI-Ly18 (DLBCL)-bearing humanized NSG mice were pretreated with 30 mg/kg Gazyva (Gpt) and treated weekly with escalating doses of CD20-TCB (0.5, 1, 2 mg/kg). Adalimumab (25 mg/kg, TNFα blockade) and tocilizumab (10 mg/kg, IL6R blockade) were given 1 day and 1 hour before the first CD20-TCB infusion. Dexamethasone (1 mg/kg) was given 1 hour prior to each therapy. Anakinra (10 mg/kg, IL1R blockade) and the NLRP3 inhibitor (20 mg/kg) were administered 1 hour before, 4 hours and 24 hours after the first CD20-TCB infusion as well as 1 hour before and 4 hours after the second CD20-TCB treatment. **A,** Bar plot representing the individual levels of cytokines in the peripheral blood 3 hours after the first CD20-TCB infusion, means of $n = 2$–5 mice/group ± SEM. Ordinary one-way ANOVA, Tukey multiple comparison test with *, $P < 0.05$; **, $P < 0.01$; ***, $P < 0.001$ and ns > 0.99. The levels of cytokines were measured in serum by Luminex. **B,** Grouped tumor growth curves, means + SEM. Two-way ANOVA on day 25 with **, $P < 0.01$ and ns > 0.99. **C,** Intratumoral $CD8^+$ T-cell count, 24 hours after third CD20-TCB infusion. Tumors were digested, and the counts of $CD8^+$ T-cells were measured by flow cytometry. Bar plots representing the maximum and minimum values for $n = 4$ mice.

and IFNγ response signaling pathways supports the early contribution of both TNFα and IFNγ in the trigger of the cytokine release cascade.

Differential gene-expression analysis revealed that transcripts of IL6, IL8, TNFα, IL1β, MCP-1, IP-10, IFNγ IL1Ra, MIP-1α, and MIP-1β are significantly induced in whole blood after treatment with CD20-TCB, highlighting their potential as CRS biomarker candidates (38). Of note, the corresponding proteins were also detected in the serum of the same whole blood assays by multiplex cytokine analysis. We conducted a more granular analysis of the scRNA-seq data to identify the cellular source and the timing of upregulation of the different cytokine genes. Although IFNγ (*IFNG*) gene was specifically expressed in T cells as of 2 hours, TNFα (*TNF*) gene was expressed in both T cells and myeloid cells at 2 hours. IL1β (*IL1B*) gene was predominantly expressed at 2 hours in monocytes and neutrophils and to a lower extent in T cells at 4 hours. IL8 (*CXCL8*) and MIP-1α (*CCL3*) genes were initially expressed at 2 hours in monocytes, then in neutrophils at 4 hours and later in T cells at 20 hours. MIP-1β (*CCL4*) gene was expressed in T cells and monocytes at 2 hours and in neutrophils at 4 hours. IL6 (*IL6*) gene was found to be specifically expressed in monocytes at 4 hours. MCP-1 (*CCL2*) gene was expressed in monocytes at 4 hours and in neutrophils and T cells at 20 hours. Finally, IP-10 (*CXCL10*) gene was expressed in monocytes, neutrophils, and T cells at 4 hours. Altogether, this shows that on-target T-cell activation (2 hours) rapidly leads to activation of neighboring and peripheral immune cells including monocytes, neutrophils, and T cells (2–20 hours). Once activated, these cells further contribute to cytokine release and amplify the inflammatory response. This highlights the importance of monitoring cytokine release at early time points during and after infusion with T-cell engagers, together with developing prophylactic mitigation strategies to prevent the instant release of proinflammatory cytokine and chemokines.

Given the central role of endothelial cells in the pathophysiology of CRS symptoms, we explored their contribution by bulk RNA-sequencing following exposure to cytokine-rich supernatants (13, 40). Endothelial cells were rapidly activated, as shown by the upregulation of ICAM1 and VCAM both at the proteomic and transcriptomic levels. At the same time, they also upregulated cytokine genes, including *IL6* and *IL1B*, and chemokine genes, including *CXCL9, CXCL10, CXCL11, CCL2, CCL5*, and *CCL8*, suggestive of their role in further amplifying the cytokine release cascade and recruiting surrounding immune cells. In line with our findings, Himmels and colleagues recently reported that cytokine and chemokines induced by T-cell–dependent bispecific

antibodies can mediate the activation of endothelial cells, which results in adhesion and infiltration of peripheral T cells in tumor and/or healthy tissues (41). Altogether, these data highlight the importance of vasculature in the safety and efficacy of T-cell–engaging therapies.

To confirm the sequence of events in the cytokine release cascade and to explore mitigation strategies of the same using clinically available molecules, we used two human model systems, including the *in vitro* whole blood assay, comprising all immune cells, and an *in vivo* model of DLBCL in immunocompetent humanized NSG mice. The *in vitro* whole blood assay allows a comprehensive assessment of the mitigation strategies on CD20-TCB–induced cytokine release, whereas the *in vivo* model of DLBCL in humanized NSG mice allows their parallel assessment of the effects on cytokine release and antitumor activity. The *in vivo* model remains limited in the assessment of cytokine release, as the proportions of myeloid cells do not match those observed in humans (42).

Our work indicates that IL6 acts as a downstream cytokine in the inflammatory cascade. Although tocilizumab is the drug of choice for the mitigation of CRS, it did not reduce CD20-TCB–induced cytokine release *in vivo* and *in vitro*, suggesting that it may prevent CRS symptoms via other mechanisms (43). Possibly, the blockade of the IL6R with tocilizumab could resolve IL6-derived toxicities, including endothelial cell activation (16). In line with previous findings, we confirmed that the prophylactic use of tocilizumab retains *in vivo* efficacy (20, 23, 38).

We demonstrated that anakinra and the NLRP3 inhibitor, which targets the upstream inflammasome pathway, attenuated myeloid cell-derived cytokine release (IL1β, MCP-1, IL6, and IL8) while retaining the antitumor efficacy *in vivo* (24). This confirmed the early contribution of IL1β in the inflammatory cascade. As shown by Norelli and colleagues and Giavridis and colleagues, the blockade of the IL1 axis may be of interest for T-cell–engaging therapies, which are associated with a risk of neurotoxicity in addition to CRS, which was mainly observed for T-cell–engaging therapies targeted against the CD19 antigen (21, 22, 44, 45).

The prophylactic blockade of TNFα with adalimumab was the most efficacious approach to reduce T-cell and myeloid cell–derived cytokines, including IL2, IL1β, IL1Ra, IP-10, IL8, MCP-1, MIP-1α, and MIP-1β confirming the upstream involvement of TNFα in mediating the cytokine release cascade. Adalimumab may prevent further activation of myeloid cells and T cells, which both express its receptors and therefore attenuate the cytokine release cascade (20). In contrast to other studies, we found that adalimumab interfered with CD20-TCB–mediated antitumor efficacy in a humanized mouse model of DLBCL. In this hematopoietic stem cell–humanized mouse model, the presence of human T cells is likely to better recapitulate the mode of action of T-cell engagers, in contrast to a transgenic mouse model, where surrogate molecules are needed (23). Further investigations revealed lower T-cell migration toward cytokine-rich supernatants from cocultures of PBMCs, tumor cells, CD20-TCB, and adalimumab. This confirms the importance of TNFα in regulating endothelial cell activation and subsequently T-cell infiltration into tumors, in line with our previous findings (3). Consequently, adalimumab may not be the preferred candidate for the prophylactic mitigation of CRS, especially for T-cell bispecific antibodies targeted against solid tumors where T-cell infiltration in the tumor plays an important role in response to treatment.

In parallel, we also investigated the effects of dexamethasone, which are widely used in the clinic to mitigate CRS (18). Dexamethasone reduced CD20-TCB–mediated cytokine release *in vitro* and prevented the cytokine elevations *in vivo* observed upon the first TCB administration. The effects of dexamethasone on efficacy differed between *in vitro* and *in vivo* settings, possibly due to the difference in their exposure in both models. Given its short *in vivo* exposure, dexamethasone only transiently interfered with T-cell activation and proliferation while efficiently reducing the cytokine release, which can cause CRS (46). This preclinical evaluation translates to recent clinical data showing that glucocorticoids did not interfere with CD20-TCB efficacy (ref. 12; ASCO 2022, Dickinson). Along those lines, the use of glucocorticoids for the management or prophylaxis of CRS was reported not to interfere with the response after treatment with the CD19xCD3 bispecific T-cell engager blinatumomab (47).

Collectively, our work contributes to the identification of the cellular and molecular players involved in cytokine and chemokine release induced by TCB treatment, together with the timing of their upregulation. We show that activated T cells initiate the cascade with the release of cytokine and chemokine, which, in turn, activate myeloid cells to amplify the cascade further. In addition to monocytes, we highlighted the role of the understudied neutrophils and endothelial cells as key mediators to the inflammatory response induced by TCBs. Targeting upstream TNFα for the mitigation of CRS may also come with a decreased T-cell infiltration and efficacy of T-cell–engaging therapies, as these play an important role in the upregulation of adhesion molecules on endothelial cells required for T-cell infiltration in the tumor (3). Our preclinical evaluation of different mitigation strategies supports the transient use of glucocorticoids for the mitigation of TCB-mediated CRS, as these potently reduce cytokine release and preserve antitumor efficacy.

Authors' Disclosures

G. Leclercq-Cohen reports personal fees from Roche Glycart outside the submitted work; in addition, G. Leclercq-Cohen has a patent related to CRS mitigation pending and a patent related to CRS mitigation issued. N. Steinhoff reports other support from Roche outside the submitted work; in addition, N. Steinhoff has a patent for P37557: NLRP3i as CRS mitigation treatment pending to Roche. L. Albertí Servera reports other support from Roche outside the submitted work. S. Nassiri reports other support from F. Hoffmann-La Roche during the conduct of the study. S. Danilin reports other support from Roche outside the submitted work. E. Piccione reports personal fees from employment with Roche and ownership of Roche stock outside the submitted work. S. Herter reports personal fees from Roche Glycart AG outside the submitted work as well as ownership of Roche stock. S. Schmeing reports other support from Roche outside the submitted work. P. Gerber reports personal fees from employment with Roche outside the submitted work. P. Schwalie reports other support from F. Hoffmann-La Roche Ltd outside the submitted work. J. Sam reports other support from Roche stocks outside the submitted work. S. Briner reports personal fees from Roche outside the submitted work. S. Jenni reports personal fees from Roche outside the submitted work. R. Bianchi reports personal fees from Roche Glycart outside the submitted work. M. Biehl reports personal fees from Roche Glycart AG outside the submitted work. F. Cremasco reports personal fees from employment with Roche and ownership of Roche stock outside the submitted work. K. Apostolopoulou reports other support from Roche Glycart AG outside the submitted work. H. Haegel reports other support from Roche outside the submitted work. C. Klein reports other support from Roche during the conduct of the study as well as other support from Roche outside the submitted work; in addition, C. Klein has a patent related to T-cell bispecifics and CRS pending and issued to Roche. P. Umaña reports other support from Roche outside the submitted work; in addition, P. Umaña has a patent for P37557 pending. M. Bacac reports various patents on Roche's T-cell bispecific antibodies issued and is an employee of Roche and own stock options of the company. No disclosures were reported by the other authors.

Authors' Contributions

G. Leclercq-Cohen: Conceptualization, data curation, formal analysis, validation, investigation, visualization, methodology, writing–original draft, project administration, writing–review and editing. **N. Steinhoff:** Conceptualization, data curation, formal analysis, validation, investigation, visualization, methodology, writing–original draft, project administration, writing–review and editing. **L. Albertí Servera:**

Conceptualization, data curation, formal analysis, investigation, visualization, methodology, writing–review and editing. **S. Nassiri:** Data curation, formal analysis, validation, visualization, writing–review and editing. **S. Danilin:** Conceptualization, data curation, software, methodology, project administration. **E. Piccione:** Data curation, formal analysis, investigation, writing–review and editing. **E. Yángüez:** Conceptualization, methodology. **T. Hüsser:** Conceptualization, methodology. **S. Herter:** Conceptualization, supervision, investigation, methodology, project administration, writing–review and editing. **S. Schmeing:** Data curation, formal analysis, writing–review and editing. **P. Gerber:** Data curation, formal analysis. **P. Schwalie:** Data curation, formal analysis. **J. Sam:** Conceptualization, supervision, investigation, methodology, project administration. **S. Briner:** Data curation. **S. Jenni:** Data curation. **R. Bianchi:** Data curation, writing–review and editing. **M. Biehl:** Data curation. **F. Cremasco:** Conceptualization, data curation, formal analysis, visualization, methodology, writing–review and editing. **K. Apostolopoulou:** Data curation, formal analysis, visualization, methodology, writing–review and editing. **H. Haegel:** Conceptualization, formal analysis, supervision, validation, investigation, methodology, project administration. **C. Klein:** Supervision, investigation, methodology, project administration, writing–review and editing. **P. Umaña:** Supervision, project administration. **M. Bacac:** Conceptualization, data curation, formal analysis, supervision, validation, investigation, visualization, methodology, writing–original draft, project administration, writing–review and editing.

Acknowledgments

The authors thank Diana Dunshee, Alessia Bottos, Sotiris Salavos, and all members of the CD20-TCB project team for critical reading of the article; all members from Cancer Immunotherapy, Oncology, Large Molecule Research, and Pharmacology at Roche Pharma Research and Early Development (pRED) or Genentech (gRED) who contributed to the studies as well as the development of the TCB program; Oncology DTA, Pharmaceutical Sciences and pRED leadership for support during all phases of the preclinical and clinical development of the program.

The publication costs of this article were defrayed in part by the payment of publication fees. Therefore, and solely to indicate this fact, this article is hereby marked "advertisement" in accordance with 18 USC section 1734.

Note

Supplementary data for this article are available at Clinical Cancer Research Online (http://clincancerres.aacrjournals.org/).

Received December 2, 2022; revised January 26, 2023; accepted June 23, 2023; published first June 28, 2023.

References

1. Bacac M, Klein C, Umana P. CEA TCB: a novel head-to-tail 2:1 T cell bispecific antibody for treatment of CEA-positive solid tumors. Oncoimmunology 2016;5:e1203498.
2. Bacac M, Fauti T, Sam J, Colombetti S, Weinzierl T, Ouaret D, et al. A novel carcinoembryonic antigen T-cell bispecific antibody (CEA TCB) for the treatment of solid tumors. Clin Cancer Res 2016;22:3286–97.
3. Bacac M, Colombetti S, Herter S, Sam J, Perro M, Chen S, et al. CD20-TCB with obinutuzumab pretreatment as next-generation treatment of hematologic malignancies. Clin Cancer Res 2018;24:4785–97.
4. Ishiguro T, Sano Y, Komatsu SI, Kamata-Sakurai M, Kaneko A, Kinoshita Y, et al. An anti-glypican 3/CD3 bispecific T cell-redirecting antibody for treatment of solid tumors. Sci Transl Med 2017;9:eaal4291.
5. Klein C, Augsberger C, Xu W, Heitmüller C, Hanisch L, Sam J, et al. Targeting intracellular WT1 in AML utilizing a T cell bispecific antibody construct: augmenting efficacy through combination with lenalidomide. Blood 2019;134(Supplement_1):4450.
6. Augsberger C, Hänel G, Xu W, Pulko V, Hanisch LJ, Augustin A, et al. Targeting intracellular WT1 in AML with a novel RMF-peptide-MHC-specific T-cell bispecific antibody. Blood 2021;138:2655–69.
7. Hutchings M, Morschhauser F, Iacoboni G, Carlo-Stella C, Offner FC, Sureda A, et al. Glofitamab, a novel, bivalent CD20-targeting T-cell-engaging bispecific antibody, induces durable complete remissions in relapsed or refractory B-cell lymphoma: a phase I trial. J Clin Oncol 2021;39:1959–70.
8. Seckinger A, Delgado JA, Moser S, Moreno L, Neuber B, Grab A, et al. Target expression, generation, preclinical activity, and pharmacokinetics of the BCMA-T cell bispecific antibody EM801 for multiple myeloma treatment. Cancer Cell 2017;31:396–410.
9. Iurlaro R, Waldhauer I, Planas-Rigol E, Bonfill-Teixidor E, Arias A, Nicolini VG, et al. A novel EGFRvIII-T cell bispecific antibody for the treatment of glioblastoma. Mol Cancer Ther 2022;21:1499–509.
10. Carlo-Stella C, Khan C, Hutchings M, Offner FC, Morschhauser F, Bachy E, et al. Glofitamab step-up dosing (SUD): updated efficacy data show high complete response rates in heavily pretreated relapsed/refractory (R/R) non-Hodgkin lymphoma (NHL) patients (Pts). Cl Lymph Myelom Leuk 2021;21:S394–S.
11. Morschhauser F, Carlo-Stella C, Offner F, Salles GA, Hutchings M, Iacoboni G, et al. Dual CD20-targeted therapy with concurrent CD20-TCB and obinutuzumab shows highly promising clinical activity and manageable safety in relapsed or refractory B-cell non-Hodgkin lymphoma: preliminary results from a phase Ib trial. Blood 2019;134:1584.
12. Dickinson MJ, Carlo-Stella C, Morschhauser F, Bachy E, Corradini P, Iacoboni G, et al. Glofitamab for relapsed or refractory diffuse large B-cell lymphoma. N Engl J Med 2022;387:2220–31.
13. Shimabukuro-Vornhagen A, Gödel P, Subklewe M, Stemmler HJ, Schlößer HA, Schlaak M, et al. Cytokine release syndrome. J Immunother Cancer. 2018;6:56.
14. Fitzgerald JC, Weiss SL, Maude SL, Barrett DM, Lacey SF, Melenhorst JJ, et al. Cytokine release syndrome after chimeric antigen receptor T cell therapy for acute lymphoblastic leukemia. Crit Care Med 2017;45:e124–e31.
15. Obstfeld AE, Frey NV, Mansfield K, Lacey SF, June CH, Porter DL, et al. Cytokine release syndrome associated with chimeric-antigen receptor T-cell therapy: clinicopathological insights. Blood 2017;130:2569–72.
16. Hay KA, Hanafi LA, Li D, Gust J, Liles WC, Wurfel MM, et al. Kinetics and biomarkers of severe cytokine release syndrome after CD19 chimeric antigen receptor-modified T-cell therapy. Blood 2017;130:2295–306.
17. Kamperschroer C, Shenton J, Lebrec H, Leighton JK, Moore PA, Thomas O. Summary of a workshop on preclinical and translational safety assessment of CD3 bispecifics. Journal of immunotoxicology 2020;17:67–85.
18. Lee DW, Santomasso BD, Locke FL, Ghobadi A, Turtle CJ, Brudno JN, et al. ASTCT consensus grading for cytokine release syndrome and neurologic toxicity associated with immune effector cells. Biol Blood Marrow Transplant 2019;25:625–38.
19. Karki R, Kanneganti TD. The 'cytokine storm': molecular mechanisms and therapeutic prospects. Trends Immunol 2021;42:681–705.
20. Leclercq G, Servera LA, Danilin S, Challier J, Steinhoff N, Bossen C, et al. Dissecting the mechanism of cytokine release induced by T-cell engagers highlights the contribution of neutrophils. OncoImmunology 2022;11:2039432.
21. Giavridis T, van der Stegen SJC, Eyquem J, Hamieh M, Piersigilli A, Sadelain M. CAR T cell-induced cytokine release syndrome is mediated by macrophages and abated by IL-1 blockade. Nat Med 2018;24:731–8.
22. Norelli M, Camisa B, Barbiera G, Falcone L, Purevdorj A, Genua M, et al. Monocyte-derived IL-1 and IL-6 are differentially required for cytokine-release syndrome and neurotoxicity due to CAR T cells. Nat Med 2018;24:739–48.
23. Li J, Piskol R, Ybarra R, Chen YJ, Li J, Slaga D, et al. CD3 bispecific antibody-induced cytokine release is dispensable for cytotoxic T cell activity. Sci Transl Med 2019;11:eaax8861.
24. Freeman TL, Swartz TH. Targeting the NLRP3 inflammasome in Severe COVID-19. Front Immunol 2020;11:1518.
25. Mädler SC, Julien-Laferriere A, Wyss L, Phan M, Sonrel A, Kang ASW, et al. Besca, a single-cell transcriptomics analysis toolkit to accelerate translational research. NAR Genomics and Bioinformatics 2021;3:lqab102.
26. Traag VA, Waltman L, van Eck NJ. From louvain to leiden: guaranteeing well-connected communities. Sci Rep 2019;9:5233.
27. Chen EY, Tan CM, Kou Y, Duan Q, Wang Z, Meirelles GV, et al. Enrichr: interactive and collaborative HTML5 gene list enrichment analysis tool. BMC Bioinf 2013;14:128.
28. Hoffman GE, Schadt EE. variancePartition: interpreting drivers of variation in complex gene expression studies. BMC Bioinf 2016;17:483.
29. Wang X, Zhao L, Wang J, Yao Y, Wang J, Ji S, et al. Correlation of cytokine release syndrome with prognosis after chimeric antigen receptor T cell therapy: analysis of 54 patients with relapsed or refractory multiple myeloma. Front Immunol 2022;13:814548.

30. Chen Y, Li R, Shang S, Yang X, Li L, Wang W, et al. Therapeutic potential of TNFα and IL1β blockade for CRS/ICANS in CAR-T therapy via ameliorating endothelial activation. Front Immunol. 2021;12:623610.
31. Hutchings M, Iacoboni G, Morschhauser F, Offner F, Sureda A, Salles GA, et al. CD20-Tcb (RG6026), a novel "2:1" format T-cell-engaging bispecific antibody, induces complete remissions in relapsed/refractory B-cell non-hodgkin's lymphoma: preliminary results from a phase i first in human trial. Blood 2018; 132:226.
32. Bacac M, Umana P, Herter S, Colombetti S, Sam J, Le Clech M, et al. CD20 Tcb (RG6026), a novel "2:1" T cell bispecific antibody for the treatment of B cell malignancies. Blood 2016;128:1836.
33. Subklewe M. BiTEs better than CAR T cells. Blood Advances 2021;5:607–12.
34. Sterner RM, Sakemura R, Cox MJ, Yang N, Khadka RH, Forsman CL, et al. GM-CSF inhibition reduces cytokine release syndrome and neuroinflammation but enhances CAR-T cell function in xenografts. Blood 2019;133:697–709.
35. Bailey SR, Vatsa S, Larson RC, Bouffard AA, Scarfo I, Kann MC, et al. Blockade or deletion of IFNg reduces macrophage activation without compromising CAR-T function in hematologic malignancies. Blood Cancer Discovery 2022;3:136–53.
36. Iwata Y, Narushima Y, Harada A, Mishima M. Priming treatment with T-cell redirecting bispecific antibody ERY974 reduced cytokine induction without losing cytotoxic activity in vitro by changing the chromatin state in T cells. Toxicol Appl Pharmacol 2022;441:115986.
37. Hernandez G, Huw L-Y, Belousov A, Wilson D, Koeppen H, McCord R, et al. Pharmacodynamic effects and immune correlates of response to the CD20/CD3 bispecific antibody mosunetuzumab in relapsed or refractory non-hodgkin lymphoma. Blood 2019;134(Supplement_1):1585.
38. Godbersen-Palmer C, Coupet TA, Grada Z, Zhang SC, Sentman CL. Toxicity induced by a bispecific T cell-redirecting protein is mediated by both T cells and myeloid cells in immunocompetent mice. J Immunol 2020;204:2973–83.
39. T. Virtanen A, Haikarainen T, Raivola J, Silvennoinen O. Selective JAKinibs: prospects in inflammatory and autoimmune diseases. BioDrugs 2019;33: 15–32.
40. Hong F, Shi M, Cao J, Wang Y, Gong Y, Gao H, et al. Predictive role of endothelial cell activation in cytokine release syndrome after chimeric antigen receptor T cell therapy for acute lymphoblastic leukaemia. J Cell Mol Med 2021;25:11063–74.
41. Himmels P, Nguyen TTT, Mitzner MC, Arrazate A, Yeung S, Burton J, et al. T cell-dependent bispecific antibodies alter organ-specific endothelial cell–T cell interaction. EMBO Rep 2023;24:e55532.
42. Tanaka S, Saito Y, Kunisawa J, Kurashima Y, Wake T, Suzuki N, et al. Development of mature and functional human myeloid subsets in hematopoietic stem cell-engrafted NOD/SCID/IL2rγKO mice. J Immunol 2012;188:6145–55.
43. Lee DW, Gardner R, Porter DL, Louis CU, Ahmed N, Jensen M, et al. Current concepts in the diagnosis and management of cytokine release syndrome. Blood 2014;124:188–95.
44. Strati P, Ahmed S, Kebriaei P, Nastoupil LJ, Claussen CM, Watson G, et al. Clinical efficacy of anakinra to mitigate CAR T-cell therapy–associated toxicity in large B-cell lymphoma. Blood Advances 2020;4:3123–7.
45. Gust J, Hay KA, Hanafi LA, Li D, Myerson D, Gonzalez-Cuyar LF, et al. Endothelial activation and blood-brain barrier disruption in neurotoxicity after adoptive immunotherapy with CD19 CAR-T Cells. Cancer Discov 2017; 7:1404–19.
46. Leclercq G, Haegel H, Toso A, Zimmermann T, Green L, Steinhoff N, et al. JAK and mTOR inhibitors prevent cytokine release while retaining T-cell bispecific antibody *in vivo* efficacy. J Immunother Cancer 2022;10:e003766.
47. Mori S, Nelson RJ, Patel RD, Ahmed WB. Low dose steroids can alleviate blinatumomab-associated toxicities without negatively impacting treatment efficacy. Blood 2015;126:4875.